Polyoxotitanium Cages

DOI: 10.1002/anie.201307721

Dipole-Induced Band-Gap Reduction in an Inorganic Cage**

Yaokang Lv, Jun Cheng, Alexander Steiner, Lihua Gan, and Dominic S. Wright**

Abstract: *Metal-doped polyoxotitanium cages are a developing class of inorganic compounds which can be regarded as nano- and sub-nano sized molecular relatives of metal-doped titania nanoparticles. These species can serve as models for the ways in which dopant metal ions can be incorporated into metal-doped titania (TiO_2), a technologically important class of photocatalytic materials with broad applications in devices and pollution control. In this study a series of cobalt(II)-containing cages in the size range ca. 0.7–1.3 nm have been synthesized and structurally characterized, allowing a coherent study of the factors affecting the band gaps in well-defined metal-doped model systems. Band structure calculations are consistent with experimental UV/Vis measurements of the Ti_xO_y absorption edges in these species and reveal that molecular dipole moment can have a profound effect on the band gap. The observation of a dipole-induced band-gap decrease mechanism provides a potentially general design strategy for the formation of low band-gap inorganic cages.*

Titanium dioxide (titania, TiO_2) is a technologically important, high band-gap semiconductor which is used in a wealth of green applications, most importantly in photocatalytic water splitting and the photocatalytic degradation of environmental pollutants.[1–3] However, because of the high band gap (ca. 3.20 eV) only the ultraviolet region of the solar radiation (< 5% of solar flux on Earth) can be harnessed in photoexcitation processes. To facilitate real-world applications using the full range of ambient sunlight it is therefore necessary to dope TiO_2 with non-metal atoms (such as N or B[4,5]) or metal ions (lanthanides[6–12] and transition metals[13–18]) which extend the absorption by the photocatalysts into visible region. Although very few studies have attempted to elucidate the way in which metal ions are incorporated into titania, it is well known that the photoactivity of metal-doped titania depends substantially on both the metal ion and its concentration[4,5] and seems to be closely related to the structure and binding mode of the dopant metal ions within titania.

Our interest in this area has focused on the exploration of a broad family of heterometallic polyoxotitanium (POT) cage compounds containing transition-metal and lanthanide ions, $[Ti_xO_y(OR)_zM_nX_m]$ (M is a dopant metal ion, X an inorganic anion).[19–24] These molecular species can be regarded as models for the incorporation of metal ions into TiO_2 and are useful as organically-soluble single-source precursors for the stoichiometrically controllable deposition of metal-doped TiO_2.[24] The cages are also of interest as organically soluble photocatalytic redox systems in organic synthesis. Herein we address the major issue of what structural and physical factors influence the band gaps in molecular transition-metal-doped POT cages. In the current study we pinpoint a new effect in the area of metal-doped POT cages, that the introduction of a large molecular dipole can induce a dramatic reduction in band gap.

The new cobalt(II)-doped POT cages $[Ti_4(OEt)_{15}O(CoBr)]$ (**1**), $[Ti_7(OEt)_{19}O_5(CoBr)]$ (**2**), $[Ti_{24}(OEt)_{30}O_{34}(CoBr)_2]$ (**3**), and $[Ti_{20}(OEt)_{23}O_{28}(Co_2I_3)(HPO_3)]$ (**4**) were obtained by the solvothermal reactions of $Ti(OR)_4$ with CoX_2 (R = Et, X = Br for **1**, **2** and **3**; R = *i*Pr, X = I for **4**) in EtOH or *i*PrOH (for **4**), by varying the reagent stoichiometries. They were characterized using a combination of elemental (C, H, and halogen) analysis, energy dispersive X-ray spectroscopy (EDS), IR spectroscopy, and positive ion electrospray mass spectrometry (see Supporting Information, Section 1). The presence of the $[HPO_3]^{2-}$ ion in **4** was traced to the 95% purity CoI_2 used in its synthesis, which elemental analysis suggests contains approximately 1.7–2.0% $[PO_4]^{3-}$. Precedents for the reduction of $[PO_4]^{3-}$ to $[HPO]_3^{2-}$ have been seen previously in a variety of transition metal cages, however, **4** is the first example found for Ti.[25]

The structural characterization of **1**–**4** by single-crystal X-ray diffraction (Figure 1) reveals a series of polyoxotitanium cages with varied Ti:Co metal compositions, whose sizes span the sub-nanometer to nanometer range (ca. 0.7–1.3 nm; see also Supporting Information Section 2). Cages **3** and **4** are the largest transition-metal-containing POT cages to be reported to date and can be regarded as nano-sized molecular relatives of cobalt(II)-doped TiO_2 nanoparticles.[26–28] The molecular arrangements in **1** and **2** are similar to those reported for the

[*] Y. Lv, Dr. J. Cheng, Prof. D. S. Wright
Department of Chemistry, University of Cambridge
Lensfield Road, Cambridge CB2 1EW (UK)
E-mail: jc590@cam.ac.uk
dsw1000@cam.ac.uk
Dr. J. Cheng
Department of Chemistry, University of Aberdeen
Aberdeen AB24 3UE (UK)
Dr. A. Steiner
Department of Chemistry, University of Liverpool
Liverpool L69 7ZD (UK)
Y. Lv, Prof. L. Gan
Department of Chemistry, Tongji University
1239 Siping Road, Shanghai 20092 (P. R. China)

[**] We thank the China Scholarship Council (Y.L.), The EU (ERC-Advanced Investigator Award D.S.W.), EPSRC (A.S.), NSFC (21273163, L.G.), Emmanuel College (Cambridge) (research fellowship for J.C.) for financial support. We also thank Prof. Michiel Sprik and Dr. Aron Cohen for helpful discussions. The calculations in this work have been performed using an allocation of computer time on HECToR, the UK's high-end computing resource funded by the Research Councils, as part of a grant to the UKCP consortium. We also thank Dr. John Davies (Cambridge, U.K.) for collecting X-ray data on **2** and **3** and for help with the refinement of data.

Supporting information for this article is available on the WWW under http://dx.doi.org/10.1002/anie.201307721.

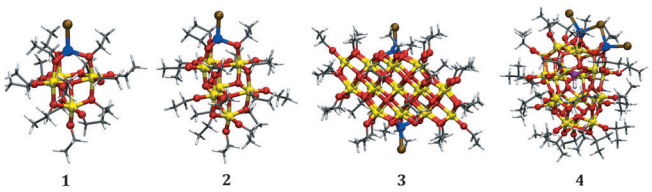

Figure 1. Single-crystal X-ray structures of $[Ti_4(OEt)_{15}O(CoBr)]$ (**1**), $[Ti_7(OEt)_{19}O_5(CoBr)]$ (**2**), $[Ti_{24}(OEt)_{30}O_{34}(CoBr)_2]$ (**3**), and $[Ti_{20}(OEt)_{23}O_{28}(Co_2I_3)(HPO_3)]$ (**4**). Ti yellow, O red, Co blue, Br or I brown, P purple. Selected bond lengths and angles can be found in the Supporting Information (caption to Figure SI-2.1).

Co^{II} chloride analogues,[19] and can be viewed as being composed of $[Ti_4(OEt)_{15}O]^-$ and $[Ti_7(OEt)_{19}O_5]^-$ ions which coordinate $[CoBr]^+$ units at the surface of the cages. The structure of **3** can be regarded in a similar way, in this case resulting from the ion-pairing of a POT dianion $[Ti_{24}(OEt)_{30}O_{34}]^{2-}$ with two $[CoBr]^+$ units which are at opposite sides of the cage. A related design principle underlies the structure of **4**, but now the two Co^{II} ions are located at one side of the oxo-titanium core within a $[Co_2I_3]^+$ fragment which is coordinated by a $[Ti_{20}(OEt)_{23}O_{28}(HPO_3)]^-$ ion, that encapsulates a phosphite ion, $[HPO_3]^{2-}$, at its center. While all of the cages have tetrahedrally coordinate Co^{2+} ions, their individual cage architectures and connectivities vary greatly. The complexes contain combinations of μ_2-, μ_3-, μ_4-, and μ_5-O oxo ligands, and exclusively six-coordinate Ti^{IV} in **1**, **2**, and **3**, and five- and six-coordinate Ti^{IV} in **4**. For comparison the three common polymorphs of TiO_2 (rutile, anatase, and brookite) have exclusively six-coordinate Ti and μ_3-O centers.[29–31]

Their structural complexity apart, the Co^{II} bromide cages **1**–**3** provide the first coherent series of transition-metal-doped cages of this type (containing the same dopant metal and halide ion), on which factors such as cage size and dopant concentration might be assessed methodically. Significant to this assessment, the degrees of condensation (i.e., the ratio of Ti to oxide ions in the cores) cover almost the entire range observed in other POT cages, from 0.25 in **1**, to 0.71 in **2**, 1.42 in **3**, and 1.40 in **4**, signifying a gradual shift in composition towards that of bulk TiO_2.[32]

The solution-state UV/Vis spectra of **1**–**3** in CH_2Cl_2 show a small but discernable red-shift in the absorption edge associated with O→Ti charge transfer within their Ti_xO_y cores in moving from the smaller cage **1** (onset at ca. 430 nm) to **2** (ca. 450 nm) and **3** (ca. 475 nm; see supporting information Figure SI-3). These absorption edges can be compared to undoped polyoxotitanium cages, which appear to be less sensitive to cage size and molecular structure, for example, $[Ti_{17}O_{24}(i\text{PrO})_{20}]$ and $[Ti_{28}O_{40}(O\text{t}\text{Bu})_{20}(OAc)_{12}]$ (ca. 350 nm for both).[33,34] It can therefore be concluded that this series of cobalt(II)-doped cages exhibits a similar trend in optical behavior as observed in cobalt(II)-doped bulk and nanoparticulate TiO_2[13–18,26,27] and that there is a trend towards increased red-shift in the absorption edge with increased cage size. However, there is clearly also a very strong structurally dependent element to the absorption edge behavior, as seen in **4** which exhibits a large red-shift in the absorption edge (ca. 530 nm). The absorption edge found in **4** is of the order of 50 nm higher than in **3**, despite the larger size of **3** and the fact that **3** contains 24 Ti rather than 20 Ti centers. Note that the observed trend in the absorption edge is roughly inversely proportional to the Co concentration in the cages, that is, **1** (5.8 wt%), **2** (4.2 wt%), **3** (3.6 wt%), and **4** (3.3 wt%). This trend, and the observed difference in absorption edges of **3** and **4**, suggests that complicated factors are at work in determining the band gaps in these species.

To understand the electronic structures of these POT cages and their UV/Vis spectra, first principles density functional theory (DFT) calculations were performed.[35] The functional of choice was hybrid B3LYP.[36] However, calculations using the GGA-PBE functional were also undertaken for comparison (see Supporting Information, Figure SI-4.1).[37] The projected B3LYP density of states (DOS) are shown in Figure 2. Although the calculated DOS are a first approximation to one-particle energy levels that correspond to (inverse) photoemission measurements, while UV/Vis spectroscopy measurements correspond to two-particle energy levels, the DOS calculations nonetheless provide a qualitative tool to understand the relative changes in the absorption spectra. The most distinct feature of the DOS plots of **1**–**4** is the appearance of new states just above the valence-band maxima (VBM) in the band gaps (labeled **i**–**v** in Figure 2). These new band-gap states can explain the experimentally observed red-shift of the adsorption edges in the region 430–530 nm, compared to comparable un-doped POT cages.

These band-gap states can be understood from the interplay of the coordination chemistry of Co^{II} complexes and the electronic band theory of POT cages. Taking cage **1** as an example, there are five clearly recognizable band-gap states labeled i–v in Figure 2a. The orbital interaction diagram is illustrated in Figure 3. The high-spin d^7 Co^{II} metal ion is at the center of a tetrahedral ligand field formed by the four p atomic orbitals (AOs) of O and Br, which leads to the conventional splitting of the Co d orbitals into bonding and anti-bonding t_2 molecular orbitals (MOs) and nonbonding e MOs. In the spin-up channel (Figure 3, left panel), most of these MOs merge with the VB of the Ti cage that mainly consists of the O 2p orbitals. The hybridization between localized states and the extended band states is often described by Anderson's impurity model in semiconductor physics which predicts that the consequence of such a hybridization is the creation of a new band-gap state near the band edges. This is exactly what is seen; a discernible state just above the VBM is produced due to the interaction between the localized MOs and the more extended band structure of the POT host, that is, state **iii** in Figure 2a, also illustrated as the dotted-line state in Figure 3 (left panel).[38] The difference between O and Br ligands breaks the degeneracy of t_2 MOs and this pushes an anti-bonding MO (state **ii**), composed largely of the Br $4p_z$ AO and a small fraction of Co 3d AO character, out of the VBM and just below the doubly degenerate Br $4p_x/4p_y$ AOs (state **i** in Figure 2a). The situation is different in the spin-down channel (Figure 3, right panel) because exchange coupling places the Co 3d orbitals at much higher energy. This leads to two major

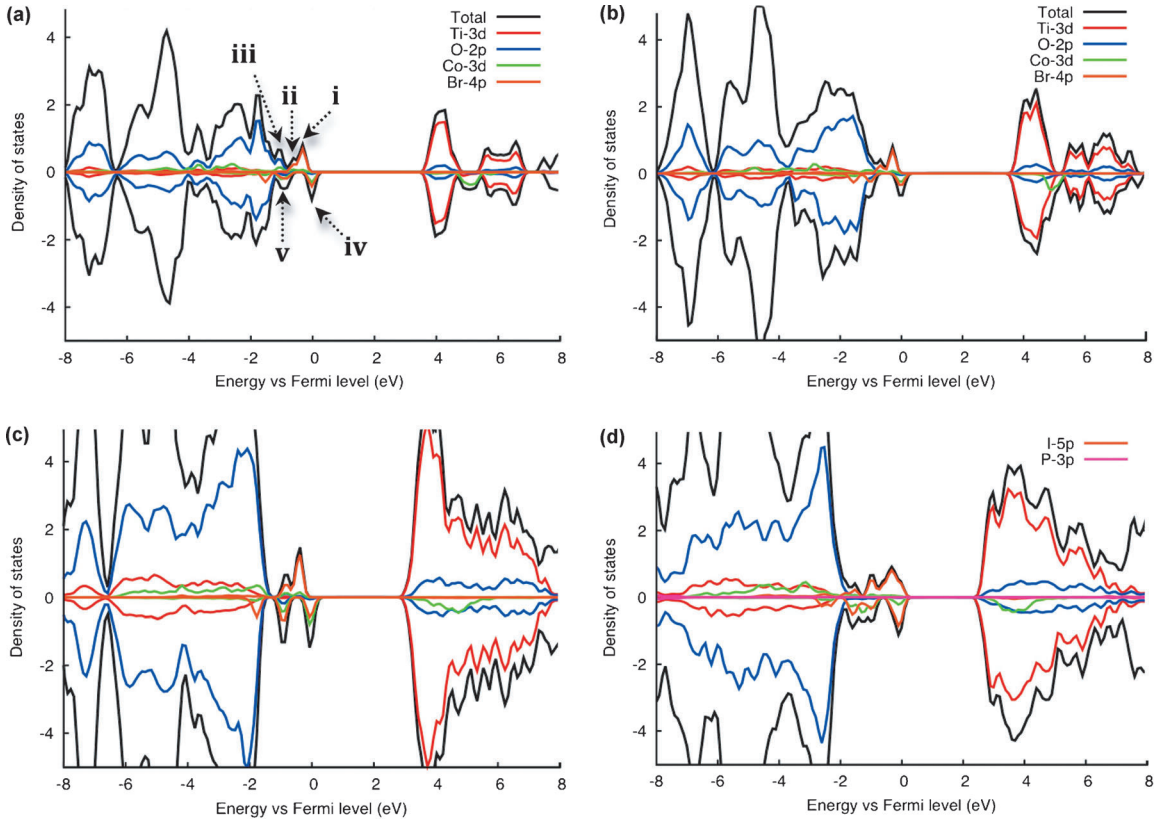

Figure 2. Plots of projected density of states calculated using B3LYP density functional, a)–d) correspond to cages **1**–**4**, respectively. Spin-up and spin-down channels are distinguished by the positive and negative signs of DOS. The five distinct band-gap states are labeled as **i**–**v** in (a). c) and d) are the DOS of the respective ferromagnetic states of cages **3** and **4**. The positions of band edges and band-gap states are listed in Table SI-4.1 in the Supporting Information. The DOS plots have also been calculated using GGA-PBE functional, and are shown in Figure SI-4.1 in Supporting Information.

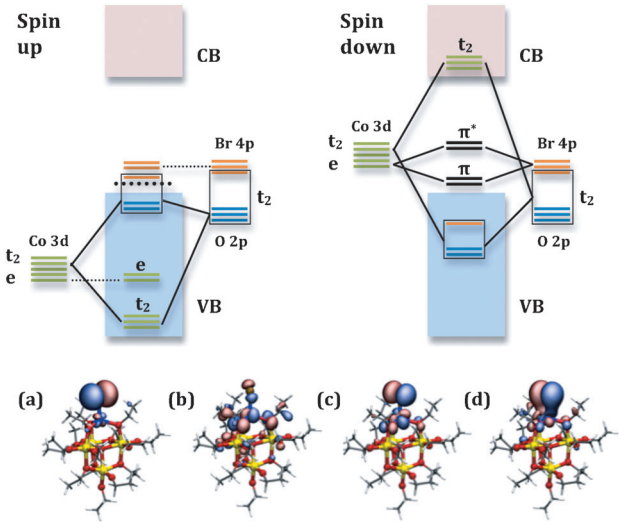

Figure 3. Orbital interaction diagram of cage **1** based on B3LYP calculations. The molecular orbitals of the band-gap states are shown in (a)–(d); a) and b) correspond to states **i** and **iii** in the spin-up channel, and c) and d) are states **iv** and **v** in the spin-down channel. See text for details.

consequences: firstly, the anti-bonding t_2 MOs now lie at much higher energy, well within the conduction band (CB) of the POT cage; secondly, the nonbonding e MOs are close to the Br $4p_x/4p_y$ AOs in energy so that they mix to form two sets of π and π* orbitals (states **iv** and **v** in Figure 2c,d).

It is now possible to understand the DOS of the other POT cages and explain the changes in their adsorption spectra. In particular, cages **1** and **2** have almost the same local structures in the region of their Co^{2+} ions (see Figure 1) except that **2** has an extra Ti_3 unit at the far end of the cage. This small structural extension marginally decreases the band gap from 5.2 to 5.1 eV, as seen in Figure 2b in which states **iii** and **v** start to merge into the VB, while keeping the positions of the rest of band-gap states essentially intact. Calculations on the previously reported Cl-substituted counterparts of **1** and **2**[18] show their band gaps are essentially the same as cages **1** and **2**, respectively, while the band-gap states slightly shift towards the VBM (see supporting information, Figure SI-4.2(a) and (b) and Table SI-4.1). Despite the difference in the coordination environment of the Co^{II} ion in **3** compared to those in **1** and **2**, that is, coordinated by μ-O ligands as opposed to OEt ligands, its DOS (Figure 2c) has very similar characteristics to **1** and **2**. The main difference is a further decrease of the band gap to 4.9 eV. The predicted red shift in the absorption edge going from **1** to **2** to **3** is in agreement with

the experimental UV/Vis data (Supporting Information Figure SI-3).

In contrast to the Ti_{24} cage **3** in which the Co^{II} ions are located on opposite sides of the molecule, in **4** the two Co^{II} ions are located on one side of the cage within a binuclear $[Co_2I_3]^+$ fragment (Figure 1). This situation still gives similar band-gap states just above the VBM as found in **3** (Figure 2d), but with a significantly smaller calculated band gap of 4.6 eV (despite the lower number of Ti atoms in **4** compared to **3**). This agrees with the observed large red-shift of the UV/Vis adsorption edge of **4** (Figure SI-3). To understand this, we notice that cage **4** can be partitioned into two sub-units which are joined by six three-coordinated O atoms: a bottom section $\{Ti_9(OiPr)_{12}O_7\}$ (which contains three six-coordinated and six five-coordinated Ti centers) and a top section $\{Ti_{11}(OiPr)_{11}O_{15}(Co_2I_3)(PO_3H)\}$ (see Figure 4a).

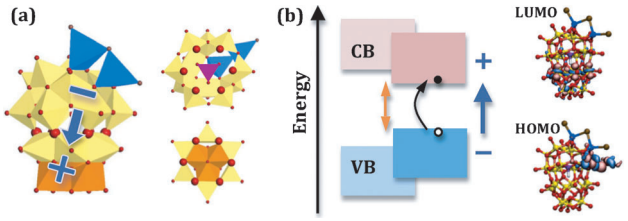

Figure 4. a) A polyhedral representation of **4** showing the charge distribution and direction of the dipole (left), the hypothetical top and bottom fragments (the six shared O-atoms between these fragments have been enlarged for clarity), and b) schematic of the dipole-induced band-gap decrease mechanism (the HOMO and LUMO are shown on the right). Ti yellow and orange polyhedra, Co blue polyhedra, O red spheres, P purple polyhedra.

Using a Mulliken population scheme it is found that the bottom section has a positive partial charge of + 0.7 e and the top section is negatively charged with the same magnitude. This charge distribution suggests the existence of an internal electric dipole pointing from the top to the bottom. This situation is confirmed by a DFT calculation which shows that **4** has a dipole moment of approximately 22 Debye in the direction shown in Figure 4a (much higher than in **1**, **2** (both ca. 9 Debye) or **3** (0 Debye)). The presence of this large dipole could potentially stabilize photo-induced electron transfer along the vector of the dipole, with a consequent reduction in the band gap. In support of this hypothesis, the highest occupied molecular orbital (HOMO) and the lowest unoccupied molecular orbital (LUMO) in **4** correspond to the VBM and conduction band minimum (CBM) of the cage, respectively, and are located at the top section and bottom section, respectively, that is, so that the HOMO→LUMO transition is in the direction of the molecular dipole. This dipole-induced band-gap reduction mechanism and the MOs involved are illustrated in Figure 4b. To further validate this mechanism, a theoretical experiment was carried out in which a slab of rutile TiO_2 was placed between a capacitor that was made up of two planes of point charges. The change in the band gap of the TiO_2 was calculated as a function of the charge of the capacitor. It is indeed found that the band gap monotonically decreases with increased charge of the capacitor (or equivalently, increased dipole moment; Figure SI-4.3).[40]

Interestingly, in a recent theoretical study of the band structures of POT cages incorporating of alkali-metal cations (Li^+ and Na^+) it was observed that a band-gap reduction occurs in these species even in the absence of mixed states at the edge of the conduction bands.[39] This result may be explainable in terms of dipole-induced decrease of the band gap, bearing in mind the asymmetric structures of the cages.

In summary, the dipole-induced decrease of the band gap is a completely novel effect in polyoxometalate or indeed in any class of inorganic cage, which may have general implications to the design of low band-gap inorganic cage molecules. The dipole-induced reduction of the band gap in **4** is in some respects analogous to band bending in semiconductor physics,[41] although unlike band bending the dipole-induced effect in **4** operates over a smaller dimension in a strong electric field rather than over spatially separated regions in a weak electric field.

Received: September 2, 2013
Revised: November 19, 2013
Published online: January 21, 2014

Keywords: band gap · cobalt · polyoxometalates · structure elucidation · titanium

[1] A. L. Linsebigler, G. Lu, J. T. Yates, *Chem. Rev.* **2009**, *109*, 735; D. O. Scanlon, C. W. Dunnill, J. Buckeridge, S. A. Shevlin, A. J. Logsdail, S. M. Woodley, C. R. A. Catlow, M. J. Powell, R. G. Palgrave, I. P. Parkin, G. W. Watson, T. W. Keal, P. Sherwood, A. Walsh, A. A. Sokol, *Nat. Mater.* **2013**, *12*, 798.
[2] R. Asahi, T. Morikawa, T. Ohwaki, K. Aoki, Y. Taga, *Science* **2001**, *293*, 269.
[3] X. Chen, L. Liu, P. Y. Yu, S. S. Mao, *Science* **2011**, *331*, 746.
[4] S. In, A. Orlov, F. García, M. Tikhov, D. S. Wright, R. M. Lambert, *Chem. Commun.* **2006**, 4236.
[5] S. In, A. Orlov, R. Berg, F. Garcia, S. Pedrosa-Jimenez, M. S. Tikhov, D. S. Wright, R. M. Lambert, *J. Am. Chem. Soc.* **2007**, *129*, 13790.
[6] M. Zalas, M. Laniecki, *Sol. Energy Mater. Sol. Cells* **2005**, *89*, 287.
[7] X. P. Cao, D. Li, W. H. Jing, W. H. Xing, Y. Q. Fan, *J. Mater. Chem.* **2012**, *22*, 15309.
[8] L. Kumaresana, A. Prabhua, M. Palanichamya, E. Arumugamb, V. Murugesana, *Hazard. Mater.* **2011**, *186*, 1183.
[9] A. Iwaszuk, M. Nolan, *Electronic J. Phys. Chem. C* **2011**, *115*, 12995.
[10] M. Sidheswaran, L. L. Tavlarides, *Ind. Eng. Chem. Res.* **2009**, *48*, 10292.
[11] L. Song, C. Chen, S. Zhang, Q. Wei, *Ultrason. Sonochem.* **2011**, *18*, 1057.
[12] K. Li, S. Wei, W. Yang, *J. Phys. Chem. Solids* **2011**, *72*, 643.
[13] M. Iwasaki, M. Hara, H. Kawada, H. Tada, S. Ito, *J. Colloid Interface Sci.* **2000**, *224*, 202.
[14] Y. Matsumoto, M. Murakami, T. Shono, T. Hasegawa, T. Fukumura, M. Kawasaki, P. Ahmet, T. Chikyow, S. Koshihara, H. Koinuma, *Science* **2001**, *291*, 854.
[15] D. Dvoranova, V. Brezova, M. Mazur, M. A. Malati, *Appl. Catal. B* **2002**, *37*, 91.
[16] K. A. Griffin, A. B. Pakhomov, C. M. Wang, S. M. Heald, K. M. Krishnan, *Phys. Rev. Lett.* **2005**, *94*, 157204.

[17] J. Choi, H. Park, M. R. Hoffmann, *J. Phys. Chem. C* **2009**, *114*, 783.
[18] J. D. Bryan, S. M. Heald, S. A. Chambers, D. R. Gamelin, *J. Am. Chem. Soc.* **2004**, *126*, 11640.
[19] S. Eslava, F. Hengesbach, M. McPartlin, D. S. Wright, *Chem. Commun.* **2010**, *46*, 4701.
[20] S. Eslava, M. McPartlin, R. I. Thomson, J. M. Rawson, D. S. Wright, *Inorg. Chem.* **2010**, *49*, 11532.
[21] S. Eslava, B. P. R. Goodwill, M. McPartlin, D. S. Wright, *Inorg. Chem.* **2011**, *50*, 5655.
[22] Y. Lv, J. Willkomm, A. Steiner, L. Gan, E. Reisner, D. S. Wright, *Chem. Sci.* **2012**, *3*, 2470.
[23] Y. Lv, J. Willkomm, M. Leskes, A. Steiner, T. C. King, L. Gan, E. Reisner, P. T. Wood, D. S. Wright, *Chem. Eur. J.* **2012**, *18*, 11867.
[24] Y. Lv, M. M. Yao, J. P. Holgad, T. Roth, A. Steiner, L. Gan, R. M. Lambert, D. S. Wright, *RSC Adv.* **2013**, *3*, 13659.
[25] For other transition-metal cages containing $[HPO_3]^{2-}$ see, U. Kortz, J. Vaissermann, R. Thouvenot, P. Gouzerh, *Inorg. Chem.* **2003**, *42*, 1135; S. Maeda, T. Goto, M. Takamoto, K. Eda, S. Himeno, H. Takahashi, T. Hori, *Inorg. Chem.* **2008**, *47*, 11197; Y. Yang, N. Li, H. Song, H. Wang, W. Chen, S. Xiang, *Chem. Mater.* **2007**, *19*, 1889; S. Langley, M. Helliwell, R. Sessoli, S. J. Teat, R. E. P. Winpenny, *Inorg. Chem.* **2008**, *47*, 497.
[26] M. A. Barakat, H. Schaeffer, G. Hayes, S. Ismat-Shah, *Appl. Catal. B* **2005**, *57*, 23.
[27] S. Maensiri, P. Laokul, J. Klinkaewnarong, *J. Magn. Magn. Mater.* **2006**, *302*, 448.
[28] J. L. Gole, S. M. Prokes, O. J. Glembocki, J. Wang, X. Qiud, C. Burda, *Nanoscale* **2010**, *2*, 1134.
[29] W. H. Baur, *Acta Crystallogr. Sect. A* **1961**, *14*, 214.
[30] W. H. Baur, A. A. Khan, *Acta Crystallogr. Sect. B* **1971**, *27*, 2133.
[31] M. Horn, C. F. Schweryfeger, E. P. Z. Meagher, *Kristallogr.* **1972**, *136*, 273.
[32] The highest value (1.56) is found in $[Ti_{18}O_{28}H(OtBu)_{17}]$, C. F. Campana, Y. Chen, V. W. Day, W. G. Klemperer, R. A. Sparks, *J. Chem. Soc. Dalton Trans.* **1996**, 691.
[33] J. B. Benedict, R. Freindorf, E. Trzop, J. Cogswell, P. Coppens, *J. Am. Chem. Soc.* **2010**, *132*, 13669.
[34] J. B. Benedict, P. Coopens, *J. Am. Chem. Soc.* **2010**, *132*, 2938.
[35] While preparing this manuscript a paper was published on the Mn^{II}-doped cage $[[Ti_{14}MnO_{14}(OH)_2(OEt)_{28}]$ in which DFT calculations were used to determine the band gap. While this study shows that there is a band gap decrease compared to undoped cages, this cage is symmetrical and size effects and (most importantly) the effect of asymmetry/dipole moment were not considered. See Y. Chen, J. Sokolow, E. Trzop, Y.-S. Chen, P. Coppens, *J. Chin. Chem. Soc.* **2013**, *60*, 887.
[36] A. D. Becke, *J. Chem. Phys.* **1993**, *98*, 5648.
[37] J. P. Perdew, K. Burke, M. Ernzerhof, *Phys. Rev. Lett.* **1996**, *77*, 3866.
[38] The Anderson Impurity Model is a Hamiltonian model that is often used to describe heavy fermion systems and Kondo insulators, see F. D. M. Haldane, P. W. Anderson, *Phys. Rev. B* **1976**, *13*, 2553.
[39] Y. Chen, E. Trzop, A. Makal, J. D. Sokolow, P. Coppens, *Inorg. Chem.* **2013**, *52*, 4750.
[40] P. Gorai, A. G. Hollister, E. G. Seebauer, *Appl. Phys. Lett.* **2013**, *103*, 141601.
[41] Z. Zhang, J. T. Yates, Jr., *Chem. Rev.* **2012**, *112*, 5520.

